

Estimating aboveground tree biomass and leaf area index in a mountain birch forest using ASTER satellite data

J. HEISKANEN

Department of Geography, University of Helsinki, P.O. Box 64, FIN-00014 University of Helsinki, Finland

(Received 1 September 2005)

Biomass and leaf area index (LAI) are important variables in many ecological and environmental applications. In this study, the suitability of visible to shortwave infrared advanced spaceborne thermal emission and reflection radiometer (ASTER) data for estimating aboveground tree and LAI in the treeline mountain birch forests was tested in northernmost Finland. The biomass and LAI of the 128 plots were surveyed, and the empirical relationships between forest variables and ASTER data were studied using correlation analysis and linear and non-linear regression analysis. The studied spectral features also included several spectral vegetation indices (SVI) and canonical correlation analysis (CCA) transformed reflectances. The results indicate significant relationships between the biomass, LAI and ASTER data. The variables were predicted most accurately by CCA transformed reflectances, the approach corresponding to the multiple regression analysis. The lowest RMSEs were 3.45 t ha^{-1} (41.0%) and $0.28 \text{ m}^2 \text{ m}^{-2}$ (37.0%) for biomass and LAI respectively. The red band was the band with the strongest correlation against the biomass and LAI. SR and NDVI were the SVIs with the strongest linear and non-linear relationships. Although the best models explained about 85% of the variation in biomass and LAI, the undergrowth vegetation and background reflectance are likely to affect the observed relationships.

1. Introduction

The birch forests cover considerable areas north of the boreal coniferous forest belt in northern Fennoscandia (Hämet-Ahti 1963, Wielgolaski 1997). Mountain birch (*Betula pubescens* ssp. *czerepanovii*) is the most common tree or scrub in the area forming the treeline both to the north and at high elevations. The mountain birch forests are subject to natural and human induced changes, which emphasise the need for monitoring the dynamics of these ecosystems. The forests are affected by the grazing and trampling of semi-domestic reindeer (Helle 2001) and defoliated regularly over vast areas by insect herbivores (Neuvonen *et al.* 2001). Mountain birch ecosystems are also likely to be affected by climate change (Skre 2001). Observations from the Swedish Scandes indicate that the birch treeline is already slowly advancing (Kullman 2000).

Biomass and leaf area index (LAI) are important variables in many ecological and environmental applications, for example, in the regional ecosystem models (Nemani *et al.* 1993, Waring and Running 1998). Accurate estimation of biomass is required

*Email: janne.heiskanen@helsinki.fi

for carbon stock accounting and monitoring (Brown 2002, Rosenqvist *et al.* 2003). LAI is defined as one half of the total leaf area per unit ground surface area (Chen and Black 1991), and it controls many biological and physical processes in the water, nutrient and carbon cycle (Waring and Running 1998).

However, there are only a few studies concerning the biomass and LAI of the mountain birch forests. Starr *et al.* (1998), Bylund and Nordell (2001) and Dahlberg *et al.* (2004) have studied the biomass proportioning of mountain birch trees, and developed allometric relationships to approximate the biomass of a tree component or the total biomass of single trees according to some more easily measured variable, such as diameter at breast height or height. The allometric relationships have been applied to estimate the biomass for the sample plots (Starr *et al.* 1998, Bylund and Nordell 2001). Furthermore, Dahlberg *et al.* (2004) presented vegetation type averaged biomass and LAI estimates. However, in addition to these studies there is also a need for regional biomass and LAI estimates.

The possibility of estimating biomass and LAI by satellite remote sensing has been investigated in several studies at various spatial scales and environments (Badhwar *et al.* 1986, Spanner *et al.* 1990, Nemani *et al.* 1993, Chen and Cihlar 1996, Fassnacht *et al.* 1997, Häme *et al.* 1997, Myneni *et al.* 1997, Turner *et al.* 1999, Brown *et al.* 2000, Brown 2001, Chen *et al.* 2002, Tomppo *et al.* 2002, Eklundh *et al.* 2003, Laidler and Treitz 2003, Stenberg *et al.* 2004). The most frequently used remote sensing data continue to be from the optical moderate resolution sensors, like Landsat Enhanced Thematic Mapper Plus (ETM+). However, few remote sensing studies have attempted to estimate biomass and LAI for mountain birch forests (Dahlberg 2001), although the studies from the boreal coniferous forests and arctic tundra are abundant. Most of the remote sensing studies concerning the mountain birch forests have concentrated on image classification (Käyhkö and Pellikka 1994, Colpaert *et al.* 2003).

Typically, the estimation of the forest variables using optical remote sensing data has been based on empirical relationships formulated between the forest variables measured in the field and satellite data, often expressed in the form of spectral vegetation indices (SVI) (table 1). In general, SVIs attempt to enhance the spectral contribution of vegetation while minimising that of the background. SVIs using some combination of red and near-infrared (NIR) reflectances, like the simple ratio (SR) and the normalised difference vegetation index (NDVI) have been particularly popular. However, the empirical relationships are affected by various factors, including canopy closure, understory vegetation and background reflectance (Spanner *et al.* 1990). A set of soil-adjusted vegetation indices have been developed to reduce the effects of the soil background reflectance (Huete 1988, Major *et al.* 1990, Qi *et al.* 1994, Rondeaux *et al.* 1996). Furthermore, some studies have stated that the inclusion of the shortwave infrared (SWIR) into the SVIs would unify different cover types and reduce the background effects (Nemani *et al.* 1993, Brown *et al.* 2000). It is obvious that the effect of the background reflectance is pronounced in the treeline, where canopy closure varies considerably (Brown 2001).

If we wish to use satellite data to map the biomass and LAI of the mountain birch forests, it is necessary to understand how these variables relate to the satellite observed reflectance. The aim of this study was to examine the potential of the visible to shortwave infrared advanced spaceborne thermal emission and reflection radiometer (ASTER) satellite data for estimating biomass and LAI in the mountain

Table 1. Spectral vegetation indices (SVIs) examined in this study. Red, NIR and SWIR correspond to ASTER bands 2, 3 and 4.

SVI	Equation	Reference
DVI	$NIR - Red$	Tucker (1979)
SR	$\frac{NIR}{Red}$	Birth and McVey (1968)
NDVI	$\frac{NIR - Red}{NIR + Red}$	Rouse <i>et al.</i> (1973)
RDVI	$\sqrt{NDVI * DVI}$	Roujean and Breon (1995)
GEMI	$\eta(1 - 0.25\eta) \frac{Red - 0.125}{1 - Red}$; $\eta = \frac{2(NIR^2 - Red^2) + 1.5 * NIR + 0.5 * Red}{NIR + Red + 0.5}$	Pinty and Verstraete (1992)
MSI	$\frac{SWIR}{NIR}$	Rock <i>et al.</i> (1986)
NDVI _c	$\frac{NIR - Red}{NIR + Red} \left(1 - \frac{SWIR - SWIR_{min}}{SWIR_{max} - SWIR_{min}}\right)$; <i>SWIR_{min}</i> and <i>SWIR_{max}</i> are the minimum and maximum reflectances observed in the field plots.	Nemani <i>et al.</i> (1993)
RSR	$\frac{NIR}{Red} \left(1 - \frac{SWIR - SWIR_{min}}{SWIR_{max} - SWIR_{min}}\right)$; <i>SWIR_{min}</i> and <i>SWIR_{max}</i> are defined as in NDVI _c	Brown <i>et al.</i> (2000)
SAVI	$(1 + L) \frac{NIR - Red}{NIR + Red + L}$; <i>L</i> was set to 0.5	Huete (1988)
OSAVI	$(1 + L) \frac{NIR - Red}{NIR + Red + L}$; <i>L</i> was set to 0.16	Rondeaux <i>et al.</i> (1996)
SAVI2	$\frac{NIR}{Red + \frac{b}{a}}$; <i>b</i> was set to 0.025 and <i>a</i> to 1.25	Major <i>et al.</i> (1990)
MSAVI2	$NIR + 0.5 - \sqrt{(NIR + 0.5)^2 - 2(NIR - Red)}$	Qi <i>et al.</i> (1994)

birch forest in northernmost Finland. The statistical relationships between the field measured biomass, LAI and ASTER satellite data were studied using correlation analysis, and models developed by linear and non-linear regression analyses. The studied spectral features included the single spectral bands, several common SVIs, and canonical correlation analysis (CCA) transformed reflectances.

ASTER data was employed because it has relatively high spatial resolution in the visible to near infrared bands, and high spectral resolution in the shortwave infrared bands (Yamaguchi *et al.* 1998). The provision of higher order data products, such as atmospherically corrected surface reflectance data, is also increasing the applicability of ASTER data (Abrams 2000). Furthermore, ASTER has been used only very little in the study of forests.

2. Materials and methods

2.1 Study area

The study area is located in the Utsjoki region, in northernmost Finland (figure 1a). The area lies north of the continuous pine forest and is characterised by subalpine mountain birch forests, gently sloping low fells and mires. In terms of vegetation the

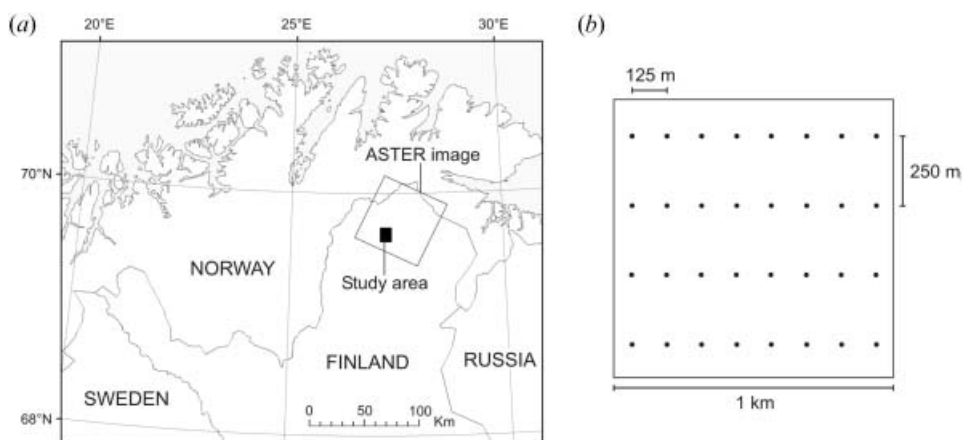


Figure 1. Location of study area (a), and sampling design of the 1 by 1 km plots (b).

study area belongs to the orohemiarctic zone, being situated at the northern boundary of the northern boreal zone (Ahti *et al.* 1968). The climate is characterised by a short growing season and long cold winters. The mean annual air temperature is -1.7°C and the mean temperature of the warmest month (July) is 13.0°C in the Kevo meteorological station situated 20 km north of the study area (Drebs *et al.* 2002). The mean annual precipitation is 414 mm. Elevations in the area range approximately from 100 to 350 m a.s.l.

The most widespread mountain birch forest types in the area are subalpine *Empetrum-Lichenes* type (sELiT), subalpine *Empetrum-Lichenes-Pleurozium* type (sELiPIT) and subalpine *Empetrum-Myrtillus* type (sEMT) (Hämet-Ahti 1963, Heikkinen and Kalliola 1988). sELiT is the driest and the most common forest type, typically occurring at greater elevations than the other types and forming almost all vertical tree lines. In the sELiT stands the birch trees or scrubs are low (2–4 m). Canopy coverage may be less than 10%, but is normally between 20–30%. In the sELiPIT and sEMT stands birches are taller (up to 6–7 m, occasionally 10 m) with canopy coverage of 30–60%.

There are also major differences in the composition of the undergrowth vegetation (Hämet-Ahti 1963, Heikkinen and Kalliola 1988). In the sELiT and sELiPIT stands the undergrowth is a mosaic of dwarf shrubs under the trees, and lichens and mosses in the patches between the trees. Dwarf birch (*Betula nana*) and Juniper (*Juniperus communis*) are the most common species in the sparse bush layer. The most abundant dwarf shrub is crowberry (*Empetrum hermaphroditum*), but also blueberry (*Vaccinium myrtillus*), cowberry (*V. vitis-idaea*) and occasionally bog bilberry (*V. uliginosum*) are present. The greater abundance of mosses in the sELiPIT (particularly *Pleurozium schreberi*) is the most important difference in comparison to sELiT. The lichens (*Cladonia*, *Stereocaulon* and *Peltigera* species) are typically very short and often disturbed by reindeer trampling. Exposed stones are also common in places. In the most luxurious sEMT stands the dwarf shrub dominated field layer and moss dominated ground layer are well developed and relatively uniform. Lichens are relatively rare. Some grasses (*Deschampsia flexuosa*, *Festuca ovina*, *Linnaea borealis*, *Solidago virgaurea* and *Trientalis europaea*) are also typically present.

2.2 Field data

The field data were surveyed in July 2004. The data were collected from four 1*1 km² study sites located in the different mountain birch forest types with variable tree and shrub covers. The study sites were chosen using the biotope inventory map and database over northernmost Finland (Sihvo 2001). The sampling design of the study sites is shown in figure 1b. Each site was surveyed by four transects located 250 m apart from each other, consisting of eight plots 125 m apart from each other. The plot size was 100 m² in the densest site and 200 m² in the three sparser sites. The centre points of the plots were located using a handheld GPS device (Magellan Meridian Platinum). According to the manufacturer the device should have an accuracy of 7 m for 95% of time. Furthermore, the GPS measurements were averaged over several minutes in order to enhance the accuracy.

The surveyed data consisted of the basic stand parameters for scrubs and trees taller than 1.3 m. Diameter at breast height (1.3 m) was measured for every tree, and height for every tenth tree. The canopy closure of the densest plots was estimated from hemispherical photographs (e.g. Rich 1990). The vegetation type and the undergrowth composition were also recorded.

The biomass of stem, live branches, dead branches and leaves were estimated using the diameter at breast height measurements and the allometric models developed for mountain birch by Starr *et al.* (1998). The biomass proportions were summed to give the aboveground tree biomass (hence called biomass). These values were converted into biomass in t ha⁻¹ using the area of the plot. The leaf area was estimated using the estimated leaf biomass and specific leaf weight (79.48 g m⁻²) measured by Kause *et al.* (1999). The estimated leaf area was converted into LAI (m² m⁻²) using the area of the plot.

Altogether 128 plots were measured in the study area, 45 plots belonging to the *sELiT* type, 56 to the *sELiPIT* type and 23 plots to the *sEMT* type. Four plots were excluded since plots were not located on mineral soils. Table 2 shows the descriptive statistics for the field data. The canopy closure of the densest plots was estimated to be around 50–60% (max=63%).

2.3 Remotely sensed data

A cloudless ASTER scene (AST_L1B.003: 2014007270) recorded on 29 July 2000 and processed into a level 2 surface reflectance (AST_07) product (Abrams 2000) was used in this study. The coverage of the image is shown in figure 1a.

Table 2. Descriptive statistics of the field data ($n=124$).

Variable	Mean	SD	Min	Max
Tree density (trees ha ⁻¹)	2709	1792	0.00	9205
Basal area (m ² ha ⁻¹)	3.11	3.08	0.00	12.38
Mean height (m)	2.85	0.74	0.00	4.96
Total tree biomass (t ha ⁻¹)	8.35	8.31	0.00	33.26
Stem biomass (t ha ⁻¹)	5.18	5.27	0.00	21.24
Live branch biomass (t ha ⁻¹)	2.41	2.36	0.00	9.51
Dead branch biomass (t ha ⁻¹)	0.16	0.16	0.00	0.65
Leaf biomass (t ha ⁻¹)	0.60	0.52	0.00	2.12
LAI (m ² m ⁻²)	0.76	0.66	0.00	2.70

SD, standard deviation.

ASTER is a high spatial resolution multispectral imager onboard NASA's Terra spacecraft, launched in December 1999 (Yamaguchi *et al.* 1998). The surface reflectance product has three spectral bands in the visible near-infrared (VNIR) and six bands in the shortwave infrared (SWIR) spectral regions with 15 and 30 metres spatial resolution, respectively (table 3). The VNIR bands were especially designed for assessing vegetation, but the spectral ranges of the SWIR bands were selected mainly for the purpose of surface soil and mineral mapping (Yamaguchi *et al.* 1998). ASTER also provides five bands in the thermal infrared (TIR) spectral region at 90 m spatial resolution, but this data were not used in this study.

The acquisition date corresponds approximately to the time of maximum leaf size. The solar zenith angle was 51°. There was a four-year lag between field work and image acquisition. However, the effect on the data analysis is assumed to be very small since biomass and LAI were estimated from the diameter at breast height, which is unlikely to have changed significantly in the four years.

2.4 Image processing

The VNIR and SWIR bands were rectified to the national coordinate system using ground control points (GCPs) and first order polynomials. The VNIR bands were rectified using 41 GCPs collected from 1 : 20 000 scale digital topographic maps. The SWIR bands were rectified using 28 GCPs collected from the rectified VNIR bands. VNIR bands were resampled to a pixel size of 15*15 m² and SWIR bands to a pixel size of 30*30 m² using nearest-neighbour resampling. The total root mean square error was 0.65 pixels (9.75 m) in the first rectification and 0.58 pixels (17.4 m) in the second.

The C-correction (Teillet *et al.* 1982, Meyer *et al.* 1993) was applied to reduce the topographically induced variations in the reflectance (r_T). The topographic correction was achieved by:

$$r_H = r_T \frac{\cos(\theta_s) + c}{\cos(i) + c} \quad (1)$$

where r_H is the reflectance observed for a horizontal surface and θ_s is the solar zenith angle. The solar incidence angle i was calculated from:

$$\cos(i) = \cos\theta_s \cos\theta_n + \sin\theta_s \sin\theta_n \cos(\phi_s - \phi_n) \quad (2)$$

Table 3. Characteristics of the ASTER visible and near-infrared (VNIR), and shortwave infrared (SWIR) subsystems (Yamaguchi *et al.* 1998).

Subsystem	Band number	Spectral range (μm)	Spatial resolution (m)
VNIR	1	0.52–0.60	15
	2	0.63–0.69	
	3	0.76–0.86	
SWIR	4	1.600–1.700	30
	5	2.145–2.185	
	6	2.185–2.225	
	7	2.235–2.285	
	8	2.295–2.365	
	9	2.360–2.430	

Table 4. Values of the parameter c employed in the topographic correction of the ASTER data, and correlation (r) between the cosine of the solar incidence angle and reflectance before and after the correction.

Band	c	r	
		Before	After
1	2.028	0.275	0.019
2	0.751	0.200	0.027
3	0.614	0.484	0.024
4	0.579	0.551	0.064
5	1.169	0.300	0.020
6	0.772	0.341	0.038
7	0.882	0.325	0.035
8	0.839	0.291	0.031
9	1.394	0.265	0.023

where θ_n is the slope of the terrain surface, ϕ_s is the solar azimuth angle and ϕ_n is the aspect of the slope. The slope and aspect were calculated from the DEM in $25 \times 25 \text{ m}^2$ pixel size. The $\cos(i)$ was resampled to match the pixel size of the VNIR and SWIR bands. The parameter c was determined by the linear regression analysis ($r_T = a \cos(i) + b$, $c = b/a$). A forest mask was derived from the biotope inventory map and slope mask ($\theta_n \geq 5$ degrees) from the DEM to limit the regression analysis to the forested and inclined pixels.

The topographic correction reduced the correlation between the solar incidence angle and surface reflectance very close to zero (table 4). This indicates that the dependence between the variables was successfully removed.

2.5 Spectral feature extraction

Plotwise reflectances were derived from the image to examine the relationship between biomass, LAI, and ASTER data. An average of reflectance inside 25 m buffer zones was calculated, and the pixel was included to the buffer zone if its midpoint was inside the border. The reflectances were determined for field plots using on average nine VNIR pixels and two SWIR pixels. The averaging was assumed to reduce the geometric errors both in the GPS measurements and in the image rectification, and furthermore, remove the difference in the pixel size between the VNIR and SWIR bands.

The reflectances were employed to calculate several frequently used SVIs (table 1). ASTER band 2 was used as a red band, band 3 as a near-infrared band and band 4 as a shortwave-infrared band in the equations. The parameters of the soil line were determined from the scatterplot of the red and near-infrared ASTER reflectances (figure 2) to calculate SAVI2 (Major *et al.* 1990). The soil line was fitted to the reflectance of the nonvegetated sandbars and stony areas. The darkest pixels correspond to the water.

2.6 Data analysis

Two-thirds of the data (83 cases) were allocated by random sampling to the modelling set and one-third (41 cases) to the validation set. The modelling set was employed to examine the linear and non-linear relationships between forest

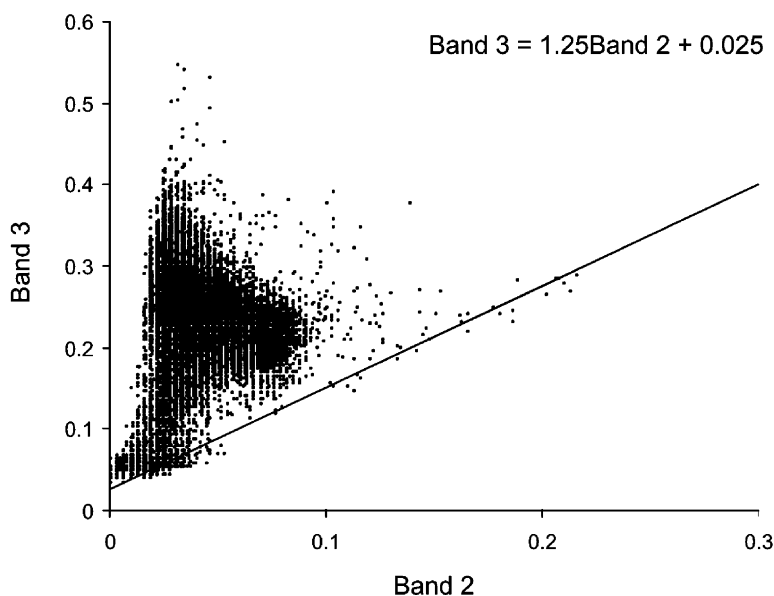


Figure 2. Scatterplot of the ASTER band 2 (red) and band 3 (near-infrared) reflectances, and the estimated soil line.

variables and spectral features using correlation analysis, and linear and non-linear regression analysis. The estimation errors were studied by the validation set.

Curran and Hay (1986) and Cohen *et al.* (2003) have stated that the ordinary least squares (OLS) regression is often an inappropriate method for relating remotely sensed data to ground variables. The problem is that OLS assumes that it is possible to specify ‘independent’ and ‘dependent’ variables, and that the independent variable is measured without error. It is difficult to make the specification and fulfil the assumptions in the case of remotely sensed data (Curran and Hay 1986). Furthermore, the predictions by the OLS tend to have attenuated variation in the direction of estimation compared to the observed values (Cohen *et al.* 2003). The reduced major axis (RMA) regression was used in this study as recommended by Curran and Hay (1986) and Cohen *et al.* (2003). The terms of the linear model ($y=ax+b$) were calculated from (Curran and Hay 1986):

$$a = \frac{\sigma_y}{\sigma_x} \quad b = \bar{y} - a\bar{x} \quad (3)$$

where \bar{y} and \bar{x} are the means of the variables y and x , and σ_y and σ_x standard deviations, respectively. The sign of the slope term a was determined from the correlation analysis. The forest variables were y and spectral features x in the analysis.

Multiple regression analysis using several spectral features is an alternative to the simple linear regression. Canonical correlation analysis (CCA) enables multiple regression analysis in a simple linear context (Cohen *et al.* 2003). CCA is a multivariate statistical procedure that allows the interrelationships between two sets of variables, in this case forest variable(s) and multispectral bands, to be investigated. CCA maximises the correlation between sets of variables and provides

a set of weights for the spectral bands that aligns them with the variation in the forest variable(s). The canonical weights can be applied to the spectral bands to give CCA scores corresponding to a single integrated index. The benefit over the multiple linear regression analysis is that the single index facilitates the visual assessment of model strength and linearity of the relationship, and enables the visualisation and interpretation on screen equally to traditional vegetation indices. Furthermore, CCA enables the use of RMA regression (Cohen *et al.* 2003).

In this study, the canonical weights were computed separately for biomass and LAI, and reflectance values were converted to the corresponding CCA scores. However, if all the spectral bands are involved in the CCA, some of the canonical weights are very small due to redundancy effects. Redundancy was minimised by selecting only the most significant variables using stepwise regression analysis before the CCA. The criterion to eliminate and include variables was that all variables in the models should be significant ($p < 0.05$). CCA scores were used in the regression analysis like all the other spectral features.

Several studies (e.g. Myneni *et al.* 1997) have reported non-linear relationships between the forest variables and reflectance data. Therefore, also the log-transformations of the ASTER bands, and the applicability of power law ($y = ax^b$) and exponential ($y = ae^{bx}$) models were examined. The models were linearised and parameters a and b estimated using RMA regression. The best type of model in terms of coefficient of determination (R^2) was chosen for each feature.

The reliability statistics included the root mean square error (RMSE), relative RMSE ($RMSE_r$), bias (Bias) and relative bias ($Bias_r$):

$$RMSE = \sqrt{\frac{\sum_{i=1}^n (\hat{y}_i - y_i)^2}{n}} \tag{4}$$

$$RMSE_r = \frac{RMSE}{\bar{y}} * 100 \tag{5}$$

$$Bias = \frac{\sum_{i=1}^n (\hat{y}_i - y_i)}{n} \tag{6}$$

$$Bias_r = \frac{Bias}{\bar{y}} * 100 \tag{7}$$

where \hat{y}_i is the estimate, y_i is the observed value, \bar{y} is the mean of the observations and n is the number of the observations (Hyvönen 2002). The statistical significance of the bias was estimated by the t -test (Ranta *et al.* 1998):

$$t = \frac{Bias}{s_D / \sqrt{n}} \tag{8}$$

where s_D is the standard deviation of the residuals ($\hat{y}_i - y_i$). The bias was considered to be significant if the absolute value of the t was greater than t corresponding to the probability of 0.05 (Hyvönen 2002).

Table 5. Correlations of the biomass and LAI against the ASTER reflectance, log-transformed ASTER reflectance, SVIs and CCA scores (n=83). All the correlations are significant ($p < 0.05$).

Band or index	Biomass	LAI
Band 1	-0.698	-0.719
Band 2	-0.831	-0.847
Band 3	0.812	0.827
Band 4	-0.821	-0.830
Band 5	-0.781	-0.798
Band 6	-0.780	-0.795
Band 7	-0.742	-0.760
Band 8	-0.730	-0.748
Band 9	-0.753	-0.771
Log (band 1)	-0.721	-0.741
Log (band 2)	-0.872	-0.883
Log (band 3)	0.792	0.810
Log (band 4)	-0.827	-0.834
Log (band 5)	-0.805	-0.819
Log (band 6)	-0.808	-0.819
Log (band 7)	-0.777	-0.792
Log (band 8)	-0.775	-0.789
Log (band 9)	-0.783	-0.798
DVI	0.834	0.850
SR	0.902	0.907
NDVI	0.817	0.835
RDVI	0.831	0.848
GEMI	0.812	0.828
MSI	-0.805	-0.823
NDVI _c	0.851	0.858
RSR	0.884	0.882
SAVI	0.832	0.849
OSAVI	0.828	0.845
SAVI2	0.888	0.897
MSAVI2	0.846	0.861
CCA scores	0.916	0.922

3. Results

3.1 Correlation between biomass, LAI and ASTER bands

All the spectral bands were significantly correlated ($p < 0.05$) with biomass and LAI (table 5). The correlation patterns were similar for both biomass and LAI due to a strong positive correlation between these two parameters ($r = 0.985$). However, the correlations were somewhat stronger with LAI than with biomass. Band 2, corresponding to the red reflectance, was the band showing the strongest correlation with biomass ($r = -0.831$) and LAI ($r = -0.847$). Also bands 3 and 4, corresponding to the NIR and SWIR reflectance, were strongly correlated with biomass and LAI. The correlation with band 3 was positive but otherwise the correlations were negative. The standard logarithmic transformation of the reflectances enhanced the correlation in all bands except in band 3. The band 2 had the strongest correlation against biomass (-0.872) and LAI (-0.883) also after the transformation.

LAI is plotted against the reflectance in bands 2, 3 and 4 in figures 3(a)–3(c). The scatterplots of the spectral bands versus biomass were very similar to those shown in figures 3(a)–3(c), and hence are not shown here. The relationship between the band 2

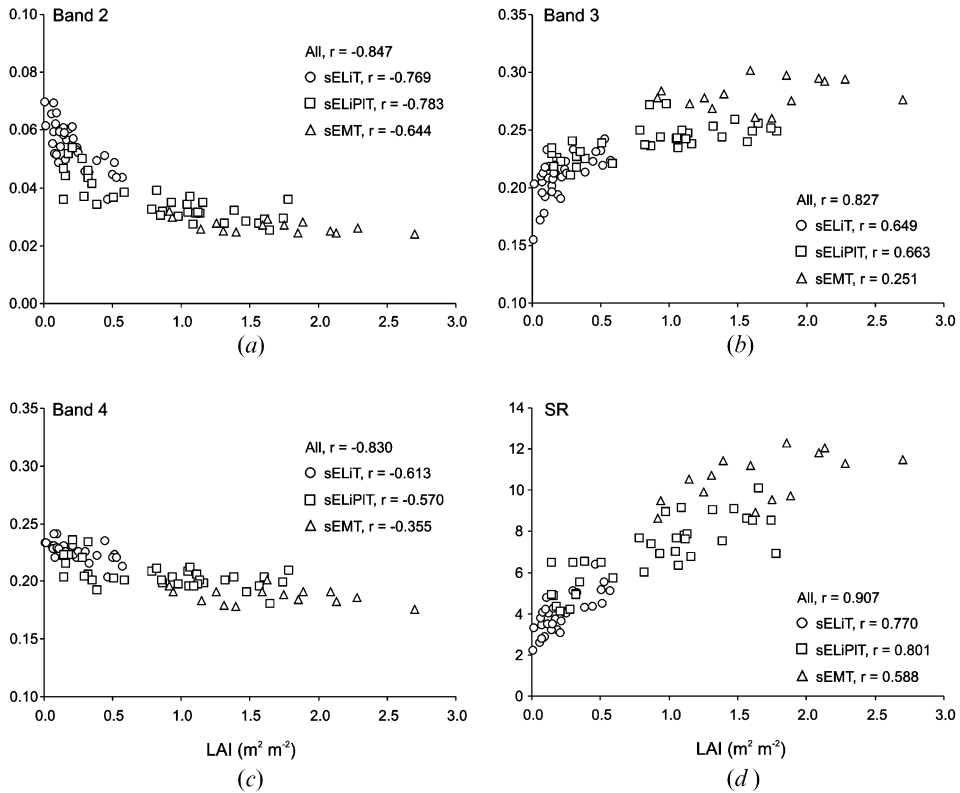


Figure 3. Relationship between LAI and ASTER band 2 (a), band 3 (b) and band 4 (c) reflectances, and relationship between LAI and SR (d). Correlation coefficients (r) are given separately for different mountain birch forest types and pooled data.

and LAI is curvilinear (figure 3(a)). The reduction in the reflectance is more rapid as LAI increases in the sparsest sELiT type compared to the denser sELiPIT and sEMT types. The relationship between band 3 and LAI is also curvilinear, because some of the sparsest sELiT sites have very low reflectance in the NIR band (figure 3(b)). Band 3 also has more scattering in the LAI values over 1 than band 2. The plots belonging to the sEMT type seem to have relatively high reflectance in band 3 compared to the other forest types. In contrast to bands 2 and 3, the relationship between band 4 and LAI is relatively linear, but reflectance in band 4 is not as sensitive to changes in LAI as reflectance in bands 2 and 3 (figure 3c). In general, all the three bands begin to saturate at LAI values of approximately 2.

Figures 3(a)–3(c) also show the forest type specific correlations for bands 2, 3 and 4, and LAI. Generally speaking, the forest type specific correlations are lower than correlations for pooled data. Band 2 is strongly correlated with LAI in all the forest types. Bands 3 and 4 show weaker correlations, particularly in the densest sEMT type. The relatively weak correlations in the sEMT type are also an indication of weak sensitivity of the bands in the high values of LAI.

3.2 Correlation between biomass, LAI and SVIs

All of the SVIs were also significantly correlated ($p < 0.05$) with biomass and LAI, SR being the SVI showing the strongest correlations, 0.902 and 0.907, respectively

(table 5). Also SAVI2 and RSR were strongly correlated with the forest variables. In comparison to the single bands, only SR and SAVI2 showed stronger correlations with biomass and LAI than the log-transformed band 2.

The LAI is plotted against SR in figure 3(d). SR shows a strong linear relation with LAI. The LAI has a stronger correlation with SR than with single bands 2 and 3, which were utilised in the calculation of SR. In the sEMT forest type the correlation is weaker with SR than with band 2 due to a very low correlation with band 3.

3.3 Canonical correlation analysis

Canonical correlation analysis was applied to convert the spectral bands into single optimised indices. According to the stepwise multiple regression analysis the bands 1, 2, 3 and 9 were employed in the CCA. Bands 1, 2 and 9 were log-transformed before the analysis, because the transformation enhanced the linear correlation. The equations to calculate the CCA scores are given in the table 6.

The CCA scores showed a stronger correlation with biomass and LAI than with single bands or SVIs, 0.916 and 0.922 respectively (table 3). The biomass and LAI are plotted against CCA scores in figure 4. The relationships are relatively linear, but the CCA scores are also insensitive to the variability in the highest biomass and LAI values. Both the pooled and forest type specific correlations are also higher than with any other feature.

Table 6. Equations to calculate CCA scores for biomass and LAI ($n=83$).

Variable	Equation
Biomass	$7.938 \text{ Log (band 1)} - 13.286 \text{ Log (band 2)} + 9.309 \text{ Band 3} + 9.953 \text{ Log (band 9)}$
LAI	$6.255 \text{ Log (band 1)} - 12.556 \text{ Log (band 2)} + 10.914 \text{ Band 3} + 10.273 \text{ Log (band 9)}$

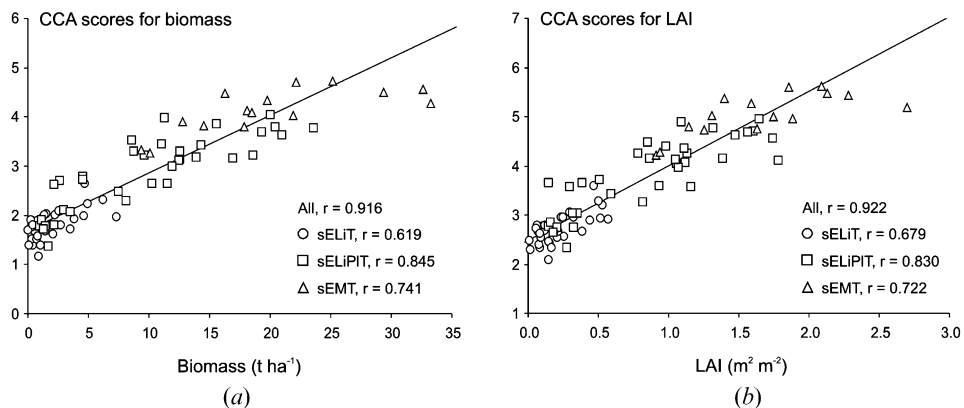


Figure 4. Relationship between biomass (a), LAI (b) and canonical correlation analysis (CCA) transformed reflectances (CCA scores). Correlation coefficients (r) are given separately for different mountain birch forest types and pooled data. The figure also shows the linear model fitted by the regression analysis.

3.4 Models for biomass and LAI

The linear regression models for biomass and LAI, and the coefficients of determination (R^2), are shown in table 7. The R^2 values of the linear models varied between 0.63 and 0.84 for biomass, and between 0.63 and 0.85 for LAI. The highest R^2 values resulted by using the CCA scores, as expected. The models for biomass and LAI using the CCA scores are shown in figure 4. The next best linear predictors of the biomass were SR ($R^2=0.81$), SAVI2 (0.79), RSR (0.78) and log (band 2) (0.76). For LAI the R^2 values were 0.82, 0.80, 0.78 and 0.78, respectively.

The non-linear regression models and R^2 values are given in table 8. In the case of band 4, SR, NDVI_c and RSR the non-linear models could not enhance the R^2 values significantly and models were not developed. However, in the case of other bands and SVIs the R^2 values were improved considerably by the non-linear models. NDVI had the highest R^2 values for both the biomass (0.85) and LAI (0.83). However, the differences to the next best models using band 2, OSAVI and SAVI were very small. The power law type models were the most common, but the exponential models produced the highest R^2 values. In contrast to the linear models, the R^2 values were slightly better for biomass than for LAI.

3.5 Error statistics

The error statistics of the linear regression models are given in table 9. The table also shows the correlation coefficients (r) between the estimated and observed biomasses and LAIs. The lowest RMSE was 3.45 t ha⁻¹ (41.0%) for biomass and 0.28 m²m⁻² (37.0%) for LAI predicted by CCA scores. The next best predictors were SR, SAVI2, RSR and log (band 2) with RMSEs between 3.63–4.08 t ha⁻¹ (43.1–48.5%) for biomass, and between 0.30–0.33 m²m⁻² (38.7–43.6%) for LAI. Also, the correlations

Table 7. Linear regression models and coefficients of determination (R^2) for biomass and LAI ($n=83$).

Band or index	Biomass (t ha ⁻¹)		LAI (m ² m ⁻²)	
	Model	R^2	Model	R^2
Band 2	-652.36x + 35.79	0.69	-50.44x + 2.86	0.72
Band 3	284.10x - 58.33	0.66	21.97x - 4.42	0.68
Band 4	-499.04x + 113.58	0.67	-38.59x + 8.87	0.69
Log (band 2)	-62.32x - 78.73	0.76	-4.82x - 6.00	0.78
Log (band 3)	152.03x + 104.59	0.63	11.76x + 8.18	0.66
Log (band 4)	-239.44x - 153.85	0.68	-18.51x - 11.81	0.70
DVI	201.94x - 30.56	0.70	15.62x - 2.27	0.72
SR	3.14x - 11.65	0.81	0.24x - 0.81	0.82
NDVI	75.74x - 43.90	0.67	5.86x - 3.31	0.70
RDVI	123.20x - 36.54	0.69	9.53x - 2.74	0.72
GEMI	165.68x - 98.68	0.66	12.81x - 7.54	0.69
MSI	-45.65x + 50.40	0.65	-3.53x + 3.99	0.68
NDVIC	36.91x - 4.44	0.72	2.85x - 0.25	0.74
RSR	2.68x - 1.34	0.78	0.21x - 0.01	0.78
SAVI	116.32x - 34.74	0.69	8.99x - 2.60	0.72
OSAVI	92.00x - 38.41	0.68	7.11x - 2.88	0.71
SAVI2	6.53x - 18.04	0.79	0.50x - 1.31	0.80
MSAVI2	104.49x - 79.84	0.72	8.08x - 6.08	0.74
CCA scores	8.54x - 14.42	0.84	0.66x - 1.64	0.85

Table 8. Non-linear regression models and coefficients of determination (R^2) for biomass and LAI ($n=83$).

Band or index	Biomass (t ha^{-1})		LAI ($\text{m}^2 \text{m}^{-2}$)	
	Model	R^2	Model	R^2
Band 2	$528.42e^{-117.53x}$	0.84	$21.37e^{-93.26x}$	0.82
Band 3	$1.28 * 10^8 x^{11.89}$	0.75	$3.99 * 10^5 x^{9.44}$	0.74
DVI	$2.34 * 10^5 x^{6.6}$	0.81	$2.69 * 10^3 x^{5.24}$	0.80
NDVI	$3.07 * 10^{-4} e^{13.64x}$	0.85	$2.41 * 10^{-4} e^{10.83x}$	0.83
RDVI	$9.1 * 10^3 x^{7.57}$	0.83	$204.45x^{6.01}$	0.81
GEMI	$1.71 * 10^4 x^{19.12}$	0.76	$336.7x^{15.18}$	0.75
MSI	$7.35 * 10^3 e^{-8.22x}$	0.81	$172.61e^{-6.53x}$	0.79
SAVI	$5.97 * 10^3 x^{7.26}$	0.83	$146.35x^{5.76}$	0.81
OSAVI	$890.63x^{7.86}$	0.84	$32.34x^{6.24}$	0.82
SAVI2	$7.47 * 10^{-3} x^{4.63}$	0.83	$3.03 * 10^{-3} x^{3.67}$	0.82
MSAVI2	$58.61x^{15.75}$	0.81	$3.73x^{12.5}$	0.80

between the estimated and observed biomasses and LAIs were strong for these features. In the case of biomass, the biases of the CCA scores, SR and RSR were negative and bias of the SAVI2 was positive. In the case of the LAI, the biases were all negative and relative biases were larger. However, the biases were not statistically significant for any of the linear models.

The biomass and LAI predicted by the CCA scores are plotted against the observed biomass and LAI values in figure 5. The estimates are strongly correlated

Table 9. Errors and biases of the biomass and LAI estimates predicted by the linear regression models, and correlations (r) between the estimated and observed biomasses and LAIs ($n=41$).

Band or index	Biomass					LAI				
	RMSE		Bias		r	RMSE		Bias		r
	t ha^{-1}	%	t ha^{-1}	%		$\text{m}^2 \text{m}^{-2}$	%	$\text{m}^2 \text{m}^{-2}$	%	
Band 2	4.71	56.0	0.36	4.3	0.833	0.37	48.3	-0.05	-6.0	0.835
Band 3	5.05	60.0	1.17	13.9	0.812	0.39	51.0	0.02	2.2	0.819
Band 4	4.87	57.9	-0.63	-7.4	0.821	0.39	51.4	-0.12	-16.0	0.815
Log (band 2)	4.08	48.5	-0.08	-0.9	0.875	0.33	42.7	-0.08	-10.5	0.873
Log (band 3)	5.28	62.8	1.31	15.6	0.793	0.41	53.2	0.03	3.6	0.801
Log (band 4)	4.79	57.0	-0.74	-8.8	0.827	0.39	50.9	-0.13	-17.2	0.819
DVI	4.70	55.8	0.94	11.1	0.836	0.36	47.5	0.00	-0.2	0.842
SR	3.63	43.1	-0.17	-2.0	0.903	0.30	38.7	-0.09	-11.5	0.897
NDVI	4.90	58.2	0.73	8.7	0.819	0.38	49.8	-0.02	-2.3	0.824
RDVI	4.72	56.1	0.85	10.1	0.833	0.37	47.8	-0.01	-1.1	0.839
GEMI	5.03	59.8	1.17	13.9	0.812	0.39	50.8	0.02	2.2	0.820
MSI	5.06	60.2	0.81	9.6	0.806	0.39	51.4	-0.01	-1.5	0.812
NDVI _c	4.42	52.6	-0.71	-8.4	0.853	0.36	47.2	-0.13	-16.9	0.845
RSR	3.97	47.2	-0.90	-10.7	0.884	0.33	43.6	-0.14	-18.8	0.870
SAVI	4.71	56.0	0.88	10.5	0.834	0.36	47.7	-0.01	-0.8	0.840
OSAVI	4.76	56.6	0.83	9.8	0.830	0.37	48.2	-0.01	-1.3	0.836
SAVI2	3.86	45.8	0.19	2.3	0.890	0.31	40.4	-0.13	-17.2	0.890
MSAVI2	4.52	53.7	0.78	9.2	0.848	0.35	45.9	-0.01	-1.8	0.853
CCA scores	3.45	41.0	-0.60	-7.2	0.913	0.28	37.0	-0.11	-14.9	0.907

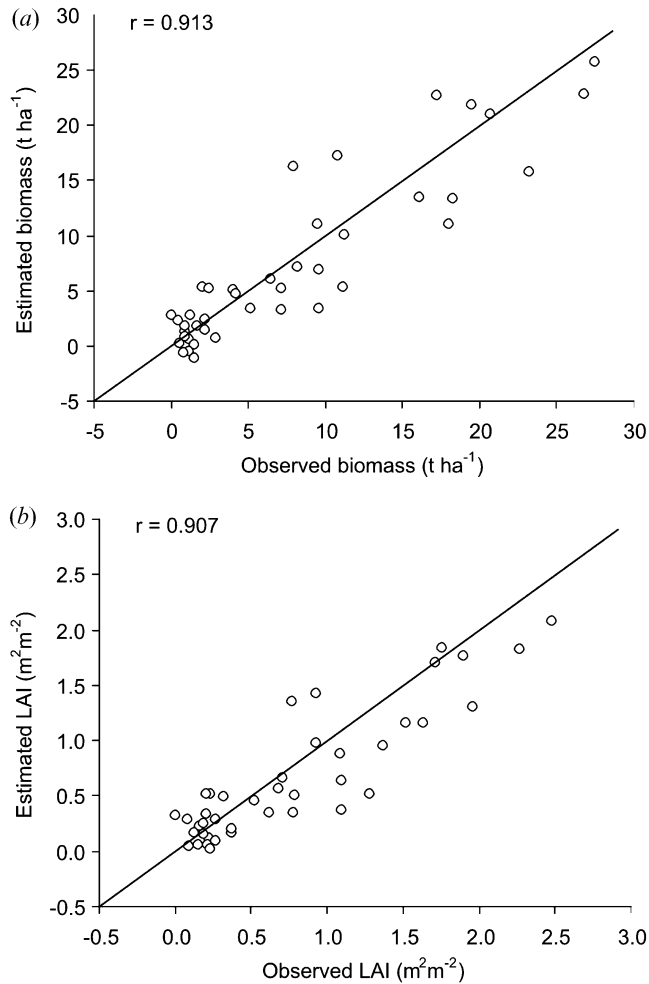


Figure 5. Estimated biomass versus observed biomass (a), and estimated LAI versus observed LAI (b). The biomass and LAI were predicted from the CCA scores.

with observed biomass and LAI, but some underprediction occurs in the high values of the variables, particularly in the case of LAI.

The error statistics of the non-linear regression models are given in table 10. Band 2 and NDVI had the smallest RMSEs for both variables and the strongest correlations between the estimated and observed values. However, the RMSEs were slightly larger and correlations weaker than those of the best linear models (table 9). In the biomass estimation the RMSE was 3.61 t ha^{-1} (45.6%) using band 2 and 4.02 t ha^{-1} (50.8%) using NDVI as predictors. The biases were negative and comparable to those of the best linear models. Some models, like GEMI and band 3 had large RMSEs and positive biases due to the overprediction in the highest biomasses. In the LAI estimation the RMSEs were $0.326 \text{ m}^2 \text{ m}^{-2}$ (42.1%) and $0.328 \text{ m}^2 \text{ m}^{-2}$ (42.4%) using band 2 and NDVI, respectively. However, band 2 and NDVI had the largest negative biases, which were also significant ($p < 0.05$).

Table 10. Errors and biases of the biomass and LAI estimates predicted by the non-linear regression models, and correlations (r) between the estimated and observed biomasses and LAIs ($n=41$).

Band or index	Biomass					LAI				
	RMSE		Bias		r	RMSE		Bias		r
	$t\ ha^{-1}$	%	$t\ ha^{-1}$	%		$m^2\ m^{-2}$	%	$m^2\ m^{-2}$	%	
Band 2	3.61	45.6	-0.70	-8.9	0.904	0.33	42.1	-0.13	-16.9	0.894
Band 3	14.16	178.9	2.85	36.0	0.731	0.73	94.9	0.06	8.3	0.770
DVI	6.97	88.1	0.75	9.5	0.815	0.43	55.1	-0.04	-5.1	0.835
NDVI	4.02	50.8	-0.36	-4.5	0.890	0.33	42.4	-0.11	-13.7	0.887
RDVI	4.84	61.2	0.03	0.3	0.858	0.35	45.5	-0.08	-10.1	0.865
GEMI	12.88	162.8	2.51	31.7	0.746	0.68	87.6	0.05	6.1	0.782
MSI	6.42	81.1	0.21	2.7	0.827	0.42	54.0	-0.08	-10.1	0.837
SAVI	5.29	66.9	0.20	2.5	0.848	0.37	47.3	-0.07	-8.9	0.858
OSAVI	4.24	53.6	-0.21	-2.7	0.874	0.34	43.6	-0.09	-11.8	0.875
SAVI2	7.34	92.8	0.68	8.6	0.839	0.43	56.1	-0.06	-7.4	0.855
MSAVI2	9.56	120.8	1.45	18.3	0.798	0.53	68.0	-0.01	-1.5	0.826

4. Discussion

4.1 Relationship between biomass, LAI and ASTER bands

Red band (band 2) was the single band with the strongest correlation with biomass and LAI. The chlorophyll pigment in the green leaves absorbs radiation in the red wavelengths and red reflectance is thus inversely related to the quantity of chlorophyll present in the canopy (Tucker and Sellers 1986). Furthermore, as canopy cover increases the amount of sunlit background decreases curvilinearly decreasing also the observed pixel-level reflectance (Yang and Prince 1997). Dahlberg (2001) reported that the red bands of the Landsat TM, SPOT XS and IRS LISS were the best predictors of the biomass and LAI in the heaths and mountain birch forests in northern Sweden. The high correlations between the red bands and forest variables has also been observed in the more productive deciduous stands (Häme *et al.* 1997, Eklundh *et al.* 2003) and in the broadleaved stands in the savannas (Xu *et al.* 2003). Furthermore, the red band has been among the most correlated bands with the forest variables in the coniferous stands (Spanner *et al.* 1990, Häme *et al.* 1997). However, Fassnacht *et al.* (1997) observed the poor performance of the red band in the hardwood forests and identified the green band to be the most correlated band with LAI in the visible range.

NIR band (band 3) showed a strong positive correlation with the forest variables. In the NIR range the leaf reflectance is high (Tucker and Sellers 1986), which increases the canopy reflectance as LAI increases. Dahlberg (2001) found that in the mountain birch forests the correlation between the NIR bands and LAI was relatively strong compared to the relationship between NIR bands and biomass. The direct relationships between NIR bands and forest variables have also been reported for other types of deciduous stands (Häme *et al.* 1997, Eklundh *et al.* 2003), in contrast to the typically inverse relationships observed in the coniferous stands (Nilson and Peterson 1994, Häme *et al.* 1997, Eklundh *et al.* 2003). Broadleaved trees with large leaves reflect effectively, but in the coniferous canopies the reflectance is reduced due to increasing multi-layer absorption as the height of the canopy increases (Häme *et al.* 1997).

SWIR band (band 4) had a strong negative correlation with biomass and LAI. This is in agreement with data from mountain birch forests (Dahlberg 2001) but in contradiction to the data from other types of deciduous stands (Eklundh *et al.* 2003). However, a strong correlation has been found between reflectance in SWIR bands and forest variables in coniferous stands (Ardö 1992, Eklundh *et al.* 2003). In the SWIR wavelengths the reflectance will decrease with increasing leaf area as a consequence of increasing absorption due to water in the canopies (Tucker and Sellers 1986). Shadowing is also likely to decrease reflectance in all bands (Ardö 1992).

4.2 Relationship between biomass, LAI and SVIs

The SR was the SVI showing the strongest linear relationship with biomass and LAI. NDVI had the strongest non-linear relationship, modelled by the exponential function. Both indices were also strongly correlated with mountain birch biomass and LAI in the study of Dahlberg (2001). Eklundh *et al.* (2003) studied the relationships between several SVIs and LAI in the more productive deciduous stands and found the strongest correlation between the SR and LAI. Broge and Leblanc (2000) compared various SVIs using the simulated canopy reflectance data and the exponential models. They found that the SR and NDVI were the best indices to estimate LAI at low and medium LAIs. The forms of the relationships are also in agreement with the results of White *et al.* (1997).

Several studies have found that SWIR modifications of the SR or NDVI improve the correlation with LAI in the coniferous forests (Nemani *et al.* 1993, Brown *et al.* 2000, Chen *et al.* 2002, Stenberg *et al.* 2004) and in the deciduous forests (Chen *et al.* 2002). However, in the comparison of Eklundh *et al.* (2003), RSR (which is the SWIR modification of the SR) performed poorly in the deciduous stands. In this study RSR showed a strong linear relationship against the forest variables, but could not enhance the correlation of the SR. The relationship was best described by the linear model in the range of biomass and LAI values observed in the mountain birch forest. However, the results of Chen *et al.* (2002) suggest that the relationship approaches exponential if higher LAI values occur. NDVI_c had a stronger linear correlation with the forest variables than NDVI, but the relationship with NDVI was better described by the exponential model. Both RSR and NDVI_c are sensitive to the MIR_{min} and MIR_{max} values used (Nemani *et al.* 1993, Brown *et al.* 2000), which is also likely to explain the differences in the model performance in the different studies.

The soil line adjusted SVIs have been employed successfully in some studies (Broge and Leblanc 2000). SAVI2 was the best predictor of LAI and the least affected index by the background reflectance in the sensitivity analysis of Broge and Leblanc (2000). In this study, SAVI2 had stronger linear relationships in comparison to other soil line adjusted SVIs, SAVI, OSAVI and MSAVI2, which were best described by the power law models. The definition of the soil line is difficult in the forested environment since the bare soil is only rarely visible and soil line is discontinuous (figure 2).

4.3 Biomass and LAI estimation using CCA scores

The strongest linear relationships in this study were observed between the biomass, LAI and CCA scores. In the case of biomass, slightly higher R^2 values were produced by some of the non-linear models, but in the case of LAI the linear model

using CCA scores also produced the highest R^2 values. According to the error statistics, the best models for both biomass and LAI were produced by the CCA scores. CCA provides a method to combine several multitemporal SVIs into a single index (Cohen *et al.* 2003), but it was also found to be useful in combining multispectral data. CCA enables the visual comparison of the single band indices with the multiple regression analysis, but it also enables the use of the RMA method in the estimation (Cohen *et al.* 2003).

The results of the CCA are comparable to the studies employing multiple regression analysis (Cohen *et al.* 2003). The results are in agreement with Fassnacht *et al.* (1997) who found that multiple-variable models offered substantial improvement over single-variable models, especially for hardwood stands. Dahlberg (2001) employed multiple regression models to map biomass and LAI in the mountain birch forests in northern Sweden. Eklundh *et al.* (2003) reported that LAI was modelled most accurately by the multiple regression models of Landsat TM bands 1, 3 and 4 also in the more productive deciduous stands.

4.4 Effect of the undergrowth vegetation and background reflectance

Several authors have emphasised the effect of the canopy closure, undergrowth vegetation and background reflectance to the observed relationships between the reflectance data and forest variables (Badhwar *et al.* 1986, Spanner *et al.* 1990, Nilson and Peterson 1994, Chen and Cihlar 1996, Yang and Prince 1997, Brown 2001). In this study, the canopy closure of the densest plots was estimated from the hemispherical photographs to be around 50–60%. Therefore, the composition of the undergrowth vegetation and background reflectance are likely to have a major effect on the observed canopy reflectance in all the studied plots, particularly in the sparsest ones.

The dwarf birch (*Betula nana*) occurred in the bush layer in most of the surveyed plots. Although the dwarf birch is a shrub (height typically from 0.2 to 0.8 m and length of the leaves from 0.5 to 1.5 cm), it is known to have spectral properties very similar to mountain birch (Käyhkö and Pellikka 1994). The dwarf birch is most abundant in the mires but it is likely to have an effect on the observed relationships and cause overprediction in the stands, where it is particularly abundant.

The spectral properties of the undergrowth vegetation differ according to the forest types. The undergrowth vegetation is particularly abundant in the sEMT type where the most important reflectors are the dwarf shrubs, grasses and mosses. This sort of undergrowth has relatively low reflectance in the red and SWIR bands but high reflectance in the NIR band (Lang *et al.* 2002). In the undergrowth of the drier sELiT type the most important reflectors are lichen and dwarf shrubs, and in the driest plots the patches of exposed soil, and partly or completely lichen covered rocks, are common. Contrary to sEMT type, this kind of undergrowth has relatively high reflectance in the red and SWIR bands and low reflectance in the NIR band (Lang *et al.* 2002). The reflectance of the undergrowth vegetation in the sELiPIT type is somewhere in between these extremes.

Hence, the reflectance of the undergrowth varies similarly to the reflectance of the mountain birch canopy in a continuum of biomass or LAI values. This will increase the correlation between the forest variables and reflectance data when data from the different forest types are combined. This was observed when the correlations of the pooled data were compared to the correlations stratified by the forest types. The

combined data also included more observations and covered a larger range of biomass and LAI values, which will increase the correlations (Chen *et al.* 2002).

The undergrowth vegetation and background reflectance are likely to affect the strength of the relationship as well as its form. In the lowest biomass and LAI values the red reflectances were high and NIR reflectances low making the relationships curvilinear. Furthermore, the sensitivity of the ASTER data to the biomass and LAI was significantly weaker in the most luxurious sEMT forest type than in the other forest types. Badhwar *et al.* (1986) found that the reflectance in all Landsat TM bands was insensitive to the overstory LAI when understory vegetation was abundant. In general, the sensitivity of the spectral data to the forest variables is the highest when the contrast between the background reflectance and canopy reflectance is greatest (Yang and Prince 1997).

There are also other possible reasons for reduced sensitivity of the spectral data in the highest biomass and LAI values. Chen *et al.* (2002) found that, in the deciduous forests, the SVIs saturate already at LAI values of 2–3 due to multiple scattering effects. In this study, the reflectance began to saturate already around biomasses of 25 t ha^{-1} and LAIs of $2 \text{ m}^2 \text{ m}^{-2}$. Furthermore, the low solar elevation angle is likely to affect the observed relationships. According to the sensitivity analysis of Yang and Prince (1997), the sensitivity of red reflectance to canopy cover variations is better with increasing solar zenith angles, but on the other hand the relationship saturates at lower canopy covers.

4.5 Applicability of the biomass and LAI models

The best models explained around 85% of the variation in the biomass and LAI values. The lowest RMSEs were 3.45 t ha^{-1} (40.97%) for biomass and $0.28 \text{ m}^2 \text{ m}^{-2}$ (36.96%) for LAI. The R^2 values reported in this study are comparable or higher in comparison to those previously reported for mountain birch (Dahlberg 2001) and other broadleaved stands (Chen *et al.* 2003, Eklundh *et al.* 2003, Xu *et al.* 2003). Generally speaking, the relative RMSEs are also comparable to the other studies, although Dahlberg (2001) has reported RMSEs as low as 21% and 12% for biomass and LAI, respectively. Keeping the accuracy of the estimates in mind, the developed regression models can be employed to estimate biomass and LAI of the mountain birch stands. The use of linear models is recommended, since non-linear models could not enhance the reliability statistics.

One reason for relatively good results is that the field plots consisted of only a single tree species, which is in contradiction to the other types of deciduous stands in the boreal or temperate zones typically consisting of multiple species (Eklundh *et al.* 2003). The biomass and LAI values were also relatively low and saturation did not affect the relationships as much as in the forest types with higher biomass and LAI. Furthermore, the relatively high spatial resolution of the VNIR bands enabled the good accuracy in the image rectification.

The most important sources of error and unexplained variation are the variable undergrowth vegetation and background (discussed above), errors in the biomass and LAI measurements, and errors in the co-registration of the image data and field plots. It is important to remember the possible overprediction, due to a high abundance of the dwarf birch, if the models are employed to predict biomass and LAI for mountain birch stands. The errors in the surveyed biomass and LAI are due to measurement errors and local deviations from the employed allometric equations and SLW value. The co-registration errors were minimised by accurate rectification

enabled by relatively high spatial resolution of the VNIR bands, and by using buffer zone averaged reflectances instead of pixelwise reflectances.

5. Conclusions

In this study, the potential of the visible to shortwave infrared satellite data for estimating biomass and LAI in mountain birch forests was examined using ASTER data. The results showed a strong statistical dependence between the biomass, LAI and satellite data. This relationship was successfully modelled by CCA and linear regression analysis. Keeping the accuracy of the estimates in mind, the developed models are applicable to estimate the biomass and LAI for mountain birch stands, and will be employed to map biomass and LAI in the study area in the future. However, the factors affecting the reflectance of mountain birch stands should be studied further by sensitivity analysis, using a suitable canopy reflectance model. Particularly, the causes of the saturation in the highest biomass and LAI values, and the effect of the undergrowth vegetation on the canopy reflectance in a continuum of canopy closure should be studied. The sensitivity analysis would also provide the optimal foundation for the selection of the most suitable SVIs for biomass and LAI estimation in mountain birch forests.

ASTER data have had only a little use in the study of forests. The widespread use of ASTER is hindered due to relatively small image size and non-systematic data collection. However, the good spatial resolution of the VNIR bands and spectral correspondence to the other optical sensors makes it a possible data source for studying forests. The bandwidths of ASTER are comparable to Landsat TM (or ETM+) in the visible and NIR spectral range. Band 4 corresponds to the TM band 5, and relatively narrow bands 5–8 correspond to TM band 7. None of the bands 5–8 were particularly sensitive to biomass or LAI in the mountain birch forests. Neither was ASTER band 9, which is outside the TM spectral range. ASTER data is also provided in the higher order data products, which reduce the effort used in completing the time consuming and often difficult pre-processing steps by the user community.

Acknowledgements

The author thanks NASA, METI, ERSDAC and LP DAAC for providing the ASTER data. The data provided by Metsähallitus was used in the field work planning and topographic correction. The field work was funded by the Finnish cultural foundation. Mrs Sonja Kivinen kindly assisted in the field work. Prof. Petri Pellikka commented on the manuscript and Mr Barnaby Clark checked the language. Also the comments of the anonymous referees were helpful to finish the paper.

References

- ABRAMS, M., 2000, The Advanced Spaceborne Thermal Emission and Reflection Radiometer (ASTER): Data products for the high spatial resolution imager on NASA's Terra platform. *International Journal of Remote Sensing*, **21**, pp. 847–859.
- AHTI, T., HÄMET-AHTI, L. and JALAS, J., 1968, Vegetation zones and their sections in northwestern Europe. *Annales Botanici Fennici*, **5**, pp. 169–211.
- ARDÖ, J., 1992, Volume quantification of coniferous forest compartments using spectral radiance recorded by Landsat Thematic Mapper. *International Journal of Remote Sensing*, **13**, pp. 1779–1786.

- BADHWAR, G.D., MACDONALD R.B., HALL, F.G. and CARNES, J.G., 1986, Spectral characterisation of biophysical characteristics in a boreal forest: Relationship between thematic mapper band reflectance and leaf area index for aspen. *IEEE Transactions on Geoscience and Remote Sensing*, **24**, pp. 322–326.
- BIRTH, G.S. and MCVY, G.R., 1968, Measuring the color of growing turf with a reflectance spectrophotometer. *Agronomy Journal*, **60**, pp. 640–643.
- BROGE, N.H. and LEBLANC, E., 2000, Comparing prediction power and stability of broadband and hyperspectral vegetation indices for estimation of green leaf area index and canopy chlorophyll density. *Remote Sensing of Environment*, **76**, pp. 156–172.
- BROWN, D.G., 2001, A spectral unmixing approach to leaf area index (LAI) estimation at the alpine treeline ecotone. In *GIS and Remote Sensing Applications in Biogeography and Ecology*, A.C. Millington, S.J. Walsh and P.E. Osbourne (Eds), pp. 7–22 (Boston: Kluwer Academic Publishers).
- BROWN, L., CHEN, J.M., LEBLANC, S.G. and CIHLAR, J., 2000, A shortwave infrared modification to the simple ratio for LAI retrieval in boreal forests: an image and model analysis. *Remote Sensing of Environment*, **71**, pp. 16–25.
- BROWN, S., 2002, Measuring carbon in forests: current status and future challenges. *Environmental Pollution*, **116**, pp. 363–372.
- BYLUND, H. and NORDELL, K.O., 2001, Biomass proportion, production and leaf nitrogen distribution in a polycormic mountain birch stand (*Betula pubescens* ssp. *czerepanovii*) in northern Sweden. In *Nordic Mountain Birch Ecosystems, Man and the Biosphere Series 27*, F.E. Wielgolaski (Ed.), pp. 115–126 (Paris: UNESCO and Carnforth: Parthenon).
- CHEN, J.M. and BLACK, T.A., 1991, Measuring leaf-area index of plant canopies with branch architecture. *Agricultural and Forest Meteorology*, **57**, pp. 1–12.
- CHEN, J.M. and CIHLAR, J., 1996, Retrieving leaf area index of boreal conifer forests using Landsat TM images. *Remote Sensing of Environment*, **55**, pp. 153–162.
- CHEN, J.M., PAVLIC, G., BROWN, L., CIHLAR, J., LEBLANC, S.G., WHITE, H.P., HALL, R.J., PEDDLE, D.R., KING, D.J., TROFYMOW, J.A., SWIFT, E., VAN DER SANDEN J. and PELLIKKA, P.K.E., 2002, Derivation and validation of Canada-wide coarse resolution leaf area index maps using high-resolution satellite imagery and ground measurements. *Remote Sensing of Environment*, **80**, pp. 165–184.
- COHEN, W.B., MAIERSPERGER, T.K., GOWER, S.T. and TURNER, D.P., 2003, An improved strategy for regression of biophysical variables and Landsat ETM+ data. *Remote Sensing of Environment*, **84**, pp. 561–571.
- COLPAERT, A., KUMPULA, J. and NIEMINEN, M., 2003, Reindeer pasture biomass assessment using satellite remote sensing. *Arctic*, **56**, pp. 147–158.
- CURRAN, P.J. and HAY, A.M., 1986, The importance of measurement error for certain procedures in remote sensing at optical wavelengths. *Photogrammetric Engineering and Remote Sensing*, **52**, pp. 229–241.
- DAHLBERG, U., 2001, Quantification and classification of Scandinavian mountain vegetation based on field data and optical satellite images. Licentiate thesis, Swedish University of Agricultural Sciences, Department of Forest Resource Management and Geomatics, Report 12.
- DAHLBERG, U., BERGE, T.W., PETERSON, H. and VENCATASAWMY, C.P., 2004, Modelling biomass and leaf area index in a sub-arctic Scandinavian mountain area. *Scandinavian Journal of Forest Research*, **19**, pp. 60–71.
- DREBS, A., NORDLUND, A., KARLSSON, P., HELMINEN, J. and RISSANEN, P., 2002, *Climatological Statistics of Finland 1971–2000*, 99 pp. (Helsinki: Finnish Meteorological Institute).
- EKLUNDH, L., HALL, K., ERIKSSON, J., ARDÖ, J. and PILESJÖ, P., 2003, Investigating the use of Landsat thematic mapper data for estimation of forest leaf area index in southern Sweden. *Canadian Journal of Remote Sensing*, **29**, pp. 349–362.

- FASSNACHT, K.S., GOWER, S.T., MACKENZIE, M.D., NORDHEIM, E.V. and LILLESAND, T.M., 1997, Estimating the leaf area index of North Central Wisconsin forests using the Landsat thematic mapper. *Remote Sensing of Environment*, **61**, pp. 229–245.
- HEIKKINEN, R.K. and KALLIOLA, R.J., 1989, Vegetation types and map of the Kevo nature reserve, northernmost Finland. *Kevo Notes*, **8**, pp. 1–39.
- HELLE, T., 2001, Mountain birch forests and reindeer husbandry. In *Nordic Mountain Birch ecosystems, Man and the Biosphere Series 27*, F.E. Wielgolaski (Ed.), pp. 279–291 (Paris: UNESCO and Carnforth: Parthenon).
- HUETE, A.R., 1988, A soil-adjusted vegetation index (SAVI). *Remote Sensing of Environment*, **25**, pp. 295–309.
- HYVÖNEN, P., 2002, Kuvioitaisten puustotunnusten ja toimenpide-ehdotusten estimointi k-lähimmän naapurin menetelmällä Landsat TM -satelliittikuvan, vanhan inventointitiedon ja kuviotason tukiaineiston avulla. *Metsätieteen aikakauskirja*, **3**, pp. 363–379 (in Finnish).
- HÄME, T., SALLI, A., ANDERSSON, K. and LOHI, A., 1997, A new methodology for the estimation of biomass of conifer-dominated boreal forest using NOAA AVHRR data. *International Journal of Remote Sensing*, **18**, pp. 3211–3243.
- HÄMET-AHTI, L., 1963, Zonation of the mountain birch forests in northernmost Fennoscandia. *Annales Botanici Societatis Zoologicae Bonaticae Fennicae 'Vanamo'*, **34**, pp. 1–127.
- MEYER, P., ITTEN, K.I., KELLENBERGER, T., SANDMEIER, S. and SANDMEIER, R., 1993, Radiometric corrections of topographically induced effects on Landsat TM data in an alpine environment. *ISPRS Journal of Photogrammetry and Remote Sensing*, **48**, pp. 17–28.
- KAUSE, A., HAUKIOJA, E. and HANHIMÄKI, S., 1999, Phenotypic plasticity in foraging behavior of sawfly larvae. *Ecology*, **80**, pp. 1230–1241.
- KULLMAN, L., 2000, Tree-limit rise and recent warming: A geoecological case study from the Swedish Scandes. *Norsk Geografisk Tidsskrift*, **54**, pp. 49–59.
- KÄYHKÖ, J. and PELLIKKA, P., 1994, Remote sensing of the impact of reindeer grazing on vegetation in northern Fennoscandia using SPOT XS data. *Polar Research*, **13**, pp. 115–124.
- LAIDLER, G.J. and TREITZ, P., 2003, Biophysical remote sensing of arctic environments. *Progress in Physical Geography*, **27**, pp. 44–68.
- LANG, M., KUUSK, A., NILSON, T., LÜKK, T., PEHK, M. and ALM, G., 2002, Reflectance spectra of ground vegetation in sub-boreal forests. Available online at: www.aai.ee/bgf/ger2600/ (accessed 6 September 2004).
- MAJOR, D.J., BARET, F. and GUYOT, G., 1990, A ratio vegetation index adjusted for soil brightness. *International Journal of Remote Sensing*, **11**, pp. 727–740.
- MYNENI, R.B., NEMANI, R.R. and RUNNING, S.W., 1997, Estimation of global leaf area index and absorbed par using radiative transfer models. *IEEE Transactions on Geoscience and Remote Sensing*, **35**, pp. 1380–1393.
- NEMANI, R., PIERCE, L., RUNNING, S. and BAND, L., 1993, Forest ecosystem processes at the watershed scale: sensitivity to remotely-sensed leaf area index estimates. *International Journal of Remote Sensing*, **14**, pp. 2519–2534.
- NEUVONEN, S., RUOHOMÄKI, K., BYLUND, H. and KAITANIEMI, P., 2001, Insect herbivores and herbivory effects on mountain birch dynamics. In *Nordic Mountain Birch Ecosystems, Man and the Biosphere Series 27*, F.E. Wielgolaski (Ed.), pp. 207–222 (Paris: UNESCO and Carnforth: Parthenon).
- NILSON, T. and PETERSON, U., 1994, Age dependence of forest reflectance: Analysis of main driving factors. *Remote Sensing of Environment*, **48**, pp. 319–331.
- PINTY, B. and VERSTRAETE, M.M., 1992, GEMI: A non-linear index to monitor global vegetation from satellites. *Vegetatio*, **101**, pp. 15–20.
- QI, J., CHEHBOUNI, A., HUETE, A.R., KERR, Y.H. and SOROOSHIAN, S., 1994, A modified soil adjusted vegetation index. *Remote Sensing of Environment*, **48**, pp. 119–126.

- RANTA, E., RITA, H. and KOUKI, J., 1999, *Biometria*, 569 pp. (Helsinki: Yliopistopaino) (in Finnish).
- RICH, P.M., 1990, Characterising plant canopies with hemispherical photographs. *Remote Sensing Reviews*, **5**, pp. 13–29.
- ROCK, B.N., VOGELMANN, J.E., WILLIAMS, D.L., VOGELMANN, A.F. and HOSHISAKI, T., 1986, Remote detection of forest damage. *BioScience*, **36**, pp. 439–445.
- RONDEAUX, G., STEVEN, M. and BARET, F., 1996, Optimisation of soil-adjusted vegetation indices. *Remote Sensing of Environment*, **55**, pp. 95–107.
- ROSENQVIST, Å., MILNE, A., LUCAS, R., IMHOFF, M. and DOBSON, C., 2003, A review of remote sensing technology in support of the Kyoto Protocol. *Environmental Science and Policy*, **6**, pp. 441–455.
- ROUJEAN, J.L. and BREON, F.M., 1995, Estimating PAR absorbed by vegetation from bidirectional reflectance measurements. *Remote Sensing of Environment*, **51**, pp. 375–384.
- ROUSE, J.W., HAAS, R.H., SCHELL, J.A. and DEERING, D.W., 1973, Monitoring vegetation systems in the Great Plains with ERTS. In *Third Earth Resources Technology Satellite-1 Symposium*, 10–14 December 1973, Washington, DC (Washington, DC: NASA), pp. 309–317.
- SIHVO, J., 2001, *Ylä-Lapin luonnonhoitoalueen ja Urho Kekkosen kansallispuiston luontokartoitus*, pp. 76 (Vantaa: Metsähallitus) (in Finnish).
- SKRE, O., 2001, Climate change impacts on mountain birch ecosystems. In *Nordic Mountain Birch Ecosystems*, Man and the biosphere series 27, F.E. Wielgolaski (Ed.), pp. 343–357 (Paris: UNESCO and Carnforth: Parthenon).
- SPANNER, M.A., PIERCE, L.L., PETERSON, D.L. and RUNNING, S.W., 1990, Remote sensing of temperate coniferous forest leaf area index. The influence of canopy closure, understory vegetation and background reflectance. *International Journal of Remote Sensing*, **11**, pp. 95–111.
- STARR, M., HARTMAN, M. and KINNUNEN, T., 1998, Biomass functions for mountain birch in the Vuoskojärvi Integrated Monitoring area. *Boreal Environment Research*, **3**, pp. 297–303.
- STENBERG, P., RAUTIAINEN, M., MANNINEN, T., VOIPIO, P. and SMOLANDER, H., 2004, Reduced simple ratio better than NDVI for estimating LAI in Finnish pine and spruce stands. *Silva Fennica*, **38**, pp. 3–14.
- TEILLET, P.M., GUINDON, B. and GOODENOUGH, D.G., 1982, On the slope-aspect correction of multispectral scanner data. *Canadian Journal of Remote Sensing*, **8**, pp. 84–106.
- TOMPPO, E., NILSON, M., ROSENBERG, M., AALTO, P. and KENNEDY, P., 2002, Simultaneous use of Landsat-TM and IRS-1C WiFS data in estimating large area tree stem volume and aboveground biomass. *Remote Sensing of Environment*, **82**, pp. 156–171.
- TUCKER, C.J., 1979, Red and photographic infrared linear combinations for monitoring vegetation. *Remote Sensing of Environment*, **8**, pp. 127–150.
- TUCKER, C.J. and SELLERS, P.J., 1986, Satellite remote sensing of primary production. *International Journal of Remote Sensing*, **7**, pp. 1395–1416.
- TURNER, D.P., COHEN, W.B., KENNEDY, R.E., FASSNACHT, K.S. and BRIGGS, J.M., 1999, Relationships between leaf area index and Landsat TM spectral vegetation indices across three temperate zone sites. *Remote Sensing of Environment*, **70**, pp. 52–68.
- WARING, R.H. and RUNNING, S.W., 1998, *Forest Ecosystems: Analysis at Multiple Scales*, 2nd edition, 370 pp. (San Diego: Academic Press).
- WIELGOLASKI, F.E., 1997, Fennoscandian tundra. In *Polar and Alpine Tundra, Ecosystems of the World 3*, F.E. Wielgolaski (Ed.), pp. 27–83 (Amsterdam: Elsevier).
- XU, B., GONG, P. and PU, R., 2003, Crown closure estimation of oak savannah in a dry season with Landsat TM imagery: comparison of various indices through correlation analysis. *International Journal of Remote Sensing*, **24**, pp. 1811–1822.

- YAMAGUCHI, Y., KAHLE, A., TSU, H., KAWAKAMI, T. and PNIEL, M., 1998, Overview of Advanced Spaceborne Thermal Emission and Reflection Radiometer (ASTER). *IEEE Transactions on Geoscience and Remote Sensing*, **36**, pp. 1062–1071.
- YANG, J. and PRINCE, S.D., 1997, A theoretical assessment of the relation between woody canopy cover and red reflectance. *Remote Sensing of Environment*, **59**, pp. 428–439.